Neuroscience Letters 785 (2022) 136724

Contents lists available at ScienceDirect

Neuroscience Letters

journal homepage: www.elsevier.com/locate/neulet

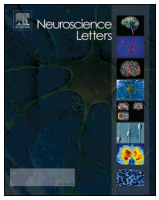

Research article

Automated quantification of brain connectivity in Alzheimer's disease using ClusterMetric

Jingqiang Wang [a,1], Caiyun Wen [b,1], Jinwen Li [a], Jianhe Chen [c,*], Yuanjing Feng [a,*]

[a] Institution of Information Processing and Automation, College of Information Engineering, Zhejiang University of Technology, Hangzhou, China
[b] The First Affiliated Hospital of Wenzhou Medical University, Wenzhou, China
[c] Wenzhou University, Wenzhou, China

ARTICLE INFO

Keywords:
Alzheimer's disease
Tractography
Fiber parcellation
ClusterMetric

ABSTRACT

Diffusion magnetic resonance imaging tractography allows investigating brain structural connections in a noninvasive way and has been widely used for understanding neurological disease. Quantification of brain connectivity along with its length by dividing a fiber bundle into multiple segments (node) is a powerful approach to assess biological properties, which is termed as tractometry. However, current tractometry methods face challenges in node identification along with the length of complex bundles whose morphology is difficult to summarize. In addition, the anatomic measure reflecting the macroscopic fiber cross-section has not been followed in previous tractometry. In this paper, we propose an automated fiber bundle quantification, which we refer to as ClusterMetric. The ClusterMetric uses a data-driven approach to identify fiber clusters corresponding to subdivisions of the white matter anatomy and identify consistent space nodes along the length of clusters across individuals. The proposed method is demonstrated by applicating to our collected dataset including 23 Alzheimer's disease (AD) patients and 22 healthy controls (HCs) and a public dataset of ADNI including 53 AD patients and 85 HCs. The altered white matter tracts in AD group are observed using both datasets, which involve several major fiber tracts including the corpus callosum, corona-radiata-frontal, arcuate fasciculus, inferior occipito-frontal fasciculus, uncinate fasciculus, thalamo-frontal, superior longitudinal fasciculus, inferior cerebellar peduncle, cingulum bundle, and extreme capsule. These fiber clusters represent the white matter connections that could be most affected in AD, suggesting the ability of our method in identifying potential abnormalities specific to local regions within a fiber cluster.

1. Introduction

Diffusion magnetic resonance imaging (dMRI) provides the technology to investigate white matter in a non-invasive way and allows the connective analysis of the living human brain [1–2]. The dMRI tractography has been widely used for identifying biological properties that are sensitive to white matter abnormalities [3–4]. Performing whole-brain tractography on the individual can generate hundreds of thousands of fibers, which makes it difficult to visually and computationally characterize brain pathways. The fibers with similar shapes and characteristics that travel together through the white matter are called fiber bundles or tracts [5]. The axons in bundles carry crucial information between cortical and/or subcortical areas. Potential damages to these bundles, e.g., neurodegeneration, can reflect in the changes of axon and myelin at the microscopic and macroscopic levels [6–7]. Therefore, grouping millions of fibers that are produced from tractogram into multiple bundles with specific functions and anatomical structures is an essential step to enable fiber pathways quantitative analysis. This process is named tractogram parcellation [8–9]. In the past decade, a plethora of white matter analytical methods combining fiber bundles with anatomical measures had been developed [10–11]. In addition, there were studies showing that white matter distortion may occur in the local position of the fiber bundle instead of the whole bundle [1012]. It was broad agreement that tractometry was a powerful analytical approach to identify local white matter changes. The white matter measures were summarized along the length of fiber tracts by dividing a fiber bundle into multiple segments (nodes). Consequently, a tractometry method commonly contained fiber parcellation, node

* Corresponding authors at: Chashan Higher Education Park, Wenzhou 325006, China (J. Chen). 288 Liuhe Road, Hangzhou 310023, China (Y. Feng).
E-mail addresses: chj@wzu.edu.cn (J. Chen), fyjing@zjut.edu.cn (Y. Feng).
[1] Caiyun Wen and Jingqiang Wang contributed equally to the study, and are co-first authors of this paper.

https://doi.org/10.1016/j.neulet.2022.136724
Received 30 January 2022; Received in revised form 26 April 2022; Accepted 8 June 2022
Available online 10 June 2022

identification, and node property measures [12–13].

As widely used tractometry methods, Automating Fiber-Tract Quantification [11–12] (AFQ) and Bundle Analytics [10] (BUAN) were computational frameworks for investigating brain pathways across populations. However, AFQ had relatively few tract definitions including hemispherical and commissural tracts. Additionally, AFQ resampled each fiber within a bundle into multiple equal distance points and the sampling points of the same orders in a bundle were viewed as a node. Though it removed some fibers that were far from the mean location for a compact bundle, it still faced challenges if the fiber bundles were divergent or fibers' lengths varied greatly. The sampling points of long fibers and the short fibers were scattered, which would make the positions of nodes within the fiber bundle ambiguous. Furthermore, it inevitably removed a lot of non-sampling points that were significant for bundle quantification. BUAN performed fiber parcellation using RecoBundles [16]. The particularly long or short fiber bundles were extracted by taking a whole-brain target tractogram as input. Then, streamline-based registration of the tractogram to MNI space was performed using an atlas of exemplar bundles (template). Moreover, the node identification within the final extracted bundles in BUAN used 'assignment' step, in which every point of the bundle was assigned to the closest point of the model centroid of atlas bundle. Though the BUAN improved the fiber parcellation and node identification compared to AFQ, it still faced challenges in the following aspects. Firstly, BUAN recognized the bundle without fine subdivisions of white matter structures, such as the corticothalamic (CT) tract. The single CT centroid was not well summarized for the morphology of thalamo-frontal (TF), thalamo-occipital (TO), and thalamo-parietal (TP), which led to confusing nodes' location on CT. In addition, the 'assignment' step was unreasonable on the large fanning bundles, such as corpus callosum (CC), which had been mentioned in BUAN. In terms of node's property measures, axon and myelination degeneration can reflect the changes of diffusion properties at the microscopic level and change of fiber bundle cross-section (FC) at the macroscopic level [17]. Diffusion tensor imaging (DTI) scale parameters were commonly used to effectively reflect the changes of axon and myelin at the microscopic level. Raffelt et al. proposed the conception of fixel to provide voxel- or local-connection-based white matter quantification [18]. As one of the fixel scale parameters, FC provided a measure for the macroscopic changes of the white matter. However, macroscopic changes such as compression and expansion along with the specific fiber bundle received no attention in previous tractometry studies.

In our work, we presented the ClusterMetric, an end-to-end computational framework (The detailed steps of ClusterMetric are shown in Fig. 1). It could identify fiber clusters with subdivisions of the white matter anatomy and summarize the anatomical measurement along with the length of cluster, as well as perform statistical analyses across groups. Our framework took a whole-brain target tractogram as input and performed data-driven whole-brain fiber parcellation and node identifications. The DTI scale parameters (FA and MD) and FC at each node were used to investigate the white matter change from the microscopic and macroscopic perspectives. The process of the proposed pipeline was as follows. Firstly, we segmented the atlas clusters into multiple nodes as a template. Secondly, the whole-brain fibers were parceled into multiple anatomical fiber clusters by using WMA algorithm [9]. According to the node template, the individual's fiber clusters in atlas space were segmented into multiple nodes. Finally, we calculated the FC, FA, and MD in individual space. The DTI parameters were got in voxels with tensor images. FC value was selected with the smallest angle with the current fiber direction in each voxel.

Furthermore, two Alzheimer's disease (AD) datasets were used to illustrate our proposed pipeline. AD was a neurodegenerative disease, which signified cognitive and memory impairments as the disease progresses [19–20]. The AD patients were commonly accompanied by white matter changes including loss of axons, demyelination, and Wallerian degeneration [21]. Our fully automated and tractogram-based approach enabled us to identify the abnormal white matter in AD at clustering level. ClusterMetric was publicly available through python scripts in https://github.com/A203-IPIS/ClusterMetric.git.

Table 1
Clinical and demographic characteristics of AD and HCs in ADNI dataset.

Variables	AD	HCs	*P*-value
Number	53	85	–
Gender (male/female)	29/24	41/44	0.76[a]
Age (Mean ± SD)	73.99 ± 7.41	73.63 ± 7.52	0.78[b]
Education year (Mean ± SD)	15.9 ± 1.66	15.7 ± 2.59	0.96[c]
MMSE (Mean ± SD)	23.39 ± 2.89	28.82 ± 1.25	less than 0.001[c]

2. Materials and methods

2.1. Participants

Data 1 The Alzheimer's Disease Neuroimaging Initiative (ADNI) dataset.

Images were obtained from the ADNI database (http://www.loni.ucla.edu/ADNI/) for 138 participants. There were 53 participants who were diagnosed with AD and 85 participants were age, sex, and education matched HCs. These AD patients received the assessment of Mini-Mental State Examination (MMSE), Alzheimer's Disease Assessment Scale13-item cognitive subscale (ADAS13), CSF, Aβ 42, t-tau measurements, and APOE genotyping. The AD patients had clinical indicts of MMSE between 11 and 26 with Clinical dementia rating (CDR) of 1. All patients met the diagnostic criteria of the National Institute of Neurological and Communicative Disorders (NINCDS) and the Stroke-Alzheimer's Disease and Related Disorders Association (ADRDA). HCs were enrolled with MMSE scores above 26 with CDR of 0, no depression, and no mild cognitive impairment or dementia. Clinical and demographic characteristics were shown in Table 1. Details about the dataset were listed as follows.

Brain images were acquired with 3 T magnetic resonance imaging (MRI) scanners. The dMRI data were obtained using the following sequence parameters: TR = 9050 *ms*, TE = 61.90 *ms*, 55 nonlinear diffusion directions with $b = 1000\ s/mm^2$ and five additional volumes with $b = 0\ s/mm^2$, matrix = 116 × 116 × 80, and voxel resolution = 2.0 *mm* × 2.0 *mm* × 2.0 *mm*, flip angle = 90^0. T1-weighted MRI data were acquired using the following parameters: TR = 2300 *ms*, TE = 2.98 *ms*, flip angle = 9^0, matrix = 256 × 256 × 170, and voxel resolution = 1.0 *mm* × 1.0 *mm* × 1.2 *mm*.

P-values labeled with [a] were obtained using Chi-square test (categorical variables) and those labeled with [b] were obtained with unpaired *t*-test (normally distributed variables), and *P*-values labeled with [c] were obtained with Mann-Whitney *U*-tests (no normally distributed variables).

Data 2 The collected dataset was from The First Affiliated Hospital of Wenzhou Medical University.

A total of 45 individuals were recruited from The First Affiliated Hospital of Wenzhou Medical University for this study including 23 AD patients and 22 age, sex, and education matched HCs. All the subjects were Chinese native speakers. Before participating in the study, written informed consent was obtained from all subjects. The study was approved by the Medical Research Ethics Committee of The First Affiliated Hospital of Wenzhou Medical University. The AD patients' inclusion criteria contained: (1) meeting the diagnostic criteria of NINCDS-ADRDA; (2) MMSE score between 11 and 26 with CDR of 1; (3) no vascular dementia and other causes of dementia. (4) Hachinski ischemic scale (HIS) total score less than 4; (5) Hamilton depression scale (HAMD) score less than 7; The HC inclusion criteria contained: (1) no abnormal behavioral ability, no history of mental and neurological diseases; (2) MMSE score more than 26; (3) no lacunar infarcts in the deep white matter; (4) no other abnormalities in routine MRI with

Table 2
Clinical and demographic characteristics of AD and HC in collected dataset.

Variables	AD	HC	*P*-value
Number	23	22	–
Gender (male/female)	10/13	8/14	0.88[a]
Age (Mean ± SD)	65.29 ± 6.88	62.90 ± 7.17	0.42[c]
Education year (Mean ± SD)	5.38 ± 3.228	6.29 ± 2.74	0.20[c]
MMSE (Mean ± SD)	17.95 ± 4.77	27.81 ± 1.53	<0.001[c]

oblique coronal hippocampal scanning; (5) Right-handedness. Details of the participants were shown in Table. 2. Details about the collected MRI data were listed as follows.

All MRI images were acquired using Philips Achieva TX 3.0 T scanner. dMRI data were obtained using the following sequence parameters: TR = 1000 *ms*, TE = 79.90 *ms*, 31 nonlinear diffusion directions with b = 800 s/mm^2 and one additional volume with $b = 0$ s/mm^2, matrix = 128 × 128 × 60, and voxel resolution = 1.72 *mm* × 1.72 *mm* × 2 *mm*, flip angle = 90^0. T1-weighted MRI data were acquired using the following parameters: TR = 25 *ms*, TE = 4.6 *ms*, matrix = 267 × 207 × 84, and voxel resolution = 0.69 *mm* × 0.69 *mm* × 1.50 *mm*.

2.2. Method overview

2.3. Process of the proposed pipeline

2.3.1. MRI data acquisition and preprocessing

The MRI dataset provided by the scanner was DICOM format, which needed to be converted into NIFTI format via DWIConvert (https://github.com/BRAINSia/BRAINSTools/tree/main/.

DWIConvert) for the subsequent processing. The denoising, head motion, and eddy current correction were conducted for dMRI data via FSL and MRtrix3 [14]. The EPI correction of dMRI data was performed using Advanced Normalization Tools [22] (ANTs) by registering to the T1-weighted MRI [8]. The output of the preprocessed data included a dMRI scan, which was well corrected and excluded the potential artifacts from the eddy current, head motion, and magnetic field distortion.

2.3.2. Whole brain fiber tractography

We conducted whole-brain tractography using a multi-fiber model to improve sensitivity in the anatomical regions of crossing fibers. The UKF method [23] fitted the mixture model of two tensors to the diffusion data

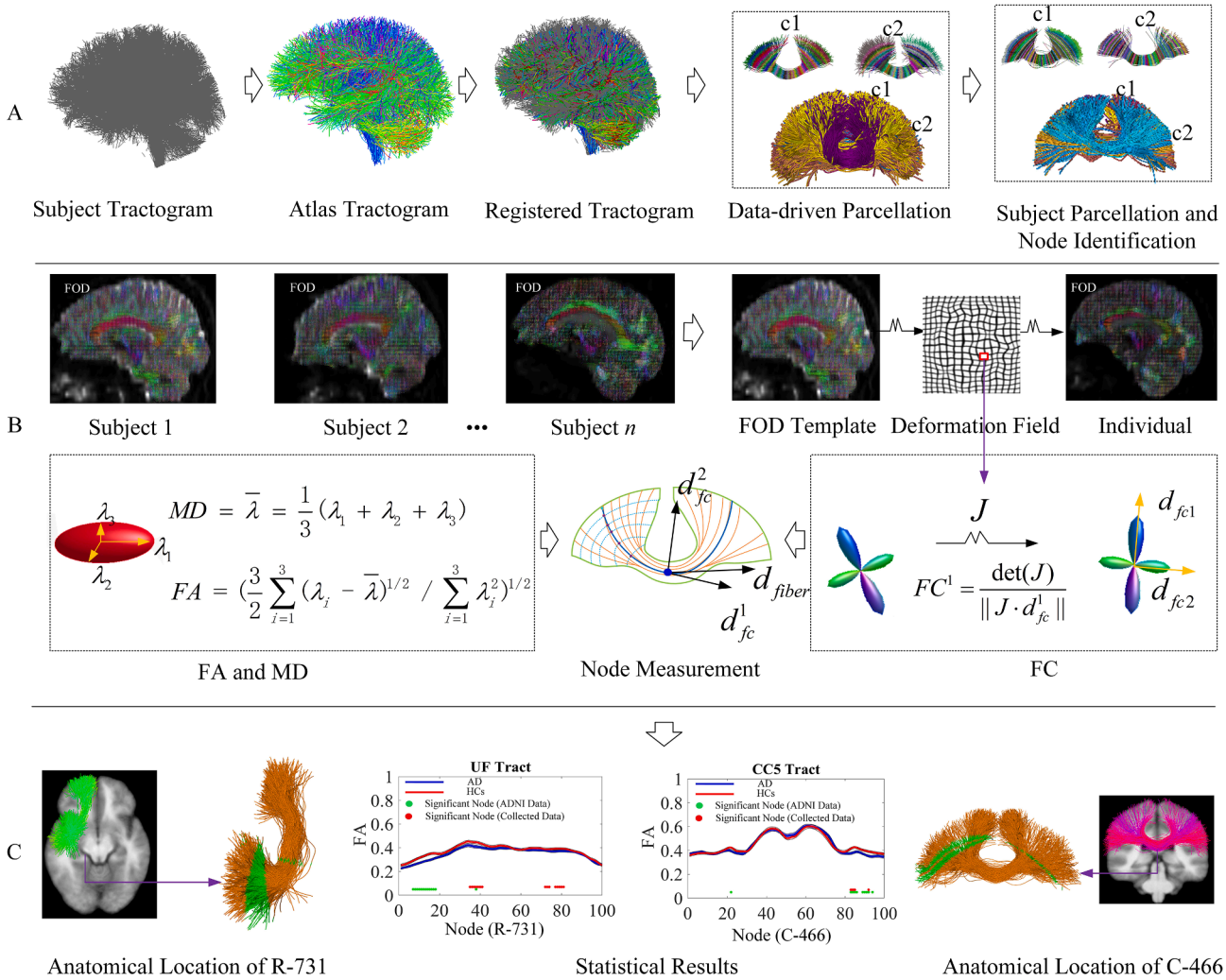

Fig. 1. Method overview: (A) Subject tractogram parcellation and node identification are performed using data-driven algorithm. (B) Node properties of FA, MD, and FC in each node are measured. FA and MD are computed from the tensor in each voxel. The FC is computed according to the Jacobian matrix J derived from deformation field from FOD template to individual's FOD. We assume an exemplar fixel containing two peaks; FC^1 is the voxel's FC measure as the fiber direction d_{fiber} has the smaller angle with d^1_{fc} compared tod^2_{fc}. (C) Statistical analysis is conducted in each node. We show two exemplar clusters with significant differences in AD compared to HCs. The green-colored locations within a bundle represent the significant regions.

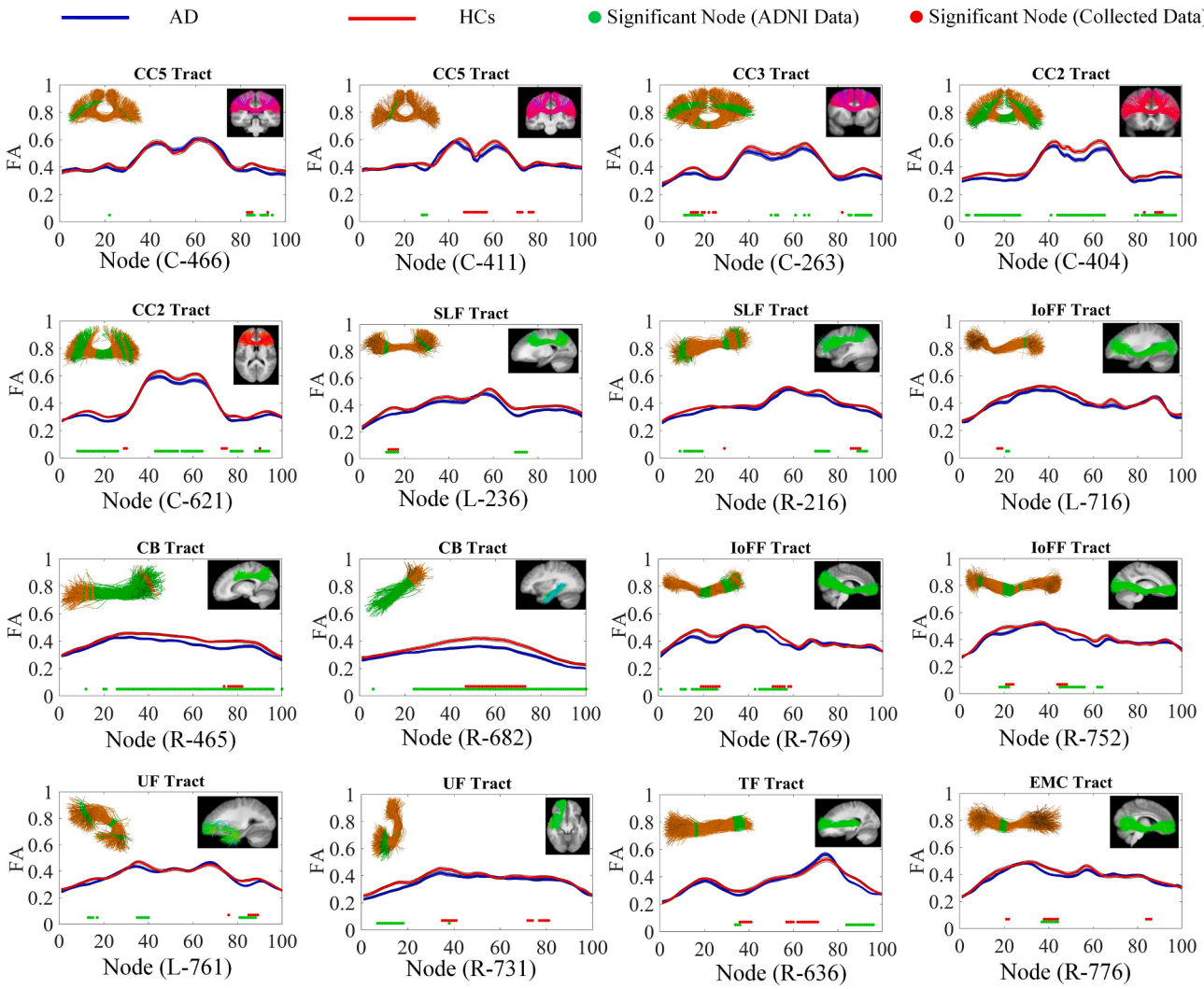

Fig. 2. Significant difference FA in AD group compared with HCs. The figure in the top left shows the corresponding cluster and the green parts within a cluster show the significant difference locations. The figures in the top right show the anatomical location of the clusters. The green dots show the significant difference nodes on ADNI dataset. The red dots show the significant difference nodes on collected dataset. The blue and red curves show the profiles of AD and HCs on ADNI dataset.

while tracking fibers (https://github.com/pnlbwh/ukftractographye), which was sensitive in the presence of crossing fibers. Moreover, each tracking step employed prior information from the previous step to help stabilize model fitting. Tractography was seeded within the binary brain mask in all voxels where FA was greater than 0.15. Tractography stopped when FA was below 0.15.

2.3.3. Fiber parcellation and node identification

We segmented each atlas cluster into multiple nodes according to the proposed ClusterMetric pipeline (details in **Supplement**). Then, we registered each subject's whole-brain tractography into atlas tractography. We transformed the registered individual's tractogram and atlas clusters to spectral embedding space. The spectral embedding for each fiber was calculated by comparing to the fibers stored in the atlas. The subject-specific white matter parcellation was then obtained by assigning the fibers to their closest atlas cluster using WMA software (https://github.com/SlicerDMRI/whitematteranalysis). We segmented each individual's cluster by assigning each point within a fiber to its closest node of template clusters. In the last step, we transformed the clusters from atlas space to individual's space. Thus, the nodes within a cluster across subjects shared the common anatomical locations, which was in accordance with the template clusters [8–9].

2.3.4. DTI scale parameters and FC calculation

Fixel-based processing steps were carried out in accordance with the fixel procedures outlined in the MRtrix3 [18] except the steps that had been done in section 2.3.1. We obtained a single unique response function to perform spherical deconvolution by averaging the response functions obtained from all subjects. Constrained spherical deconvolution (CSD) algorithm was used to produce FODs with the unique white matter response function using the dwi2fodthe dwi2fod script. Then, we selected part of the subject's FODs to generate a study-specific population unbiased FOD template [1724]. The mapping from template image to individual image can be seen as a normalized process. The Jacobian matrix J can describe the local affine transformation of this non-linear warp. The determinant of J can assess the overall white matter volume change in a voxel along the fixel's direction. Expansion or contraction in the perpendicular plane reflected the differences in the number of axons [18]. We computed the FC as the formula:$FC^i = \det(J)/||J \cdot d^i_{fc}||$. The d^i_{fc} was the unit peak direction of FOD template in current voxel, which was pre-defined in fixel mask template in individual's space. Note that FC was estimated (warp2metric script in MRtrix3) using the warp field that mapped from individual to template space.

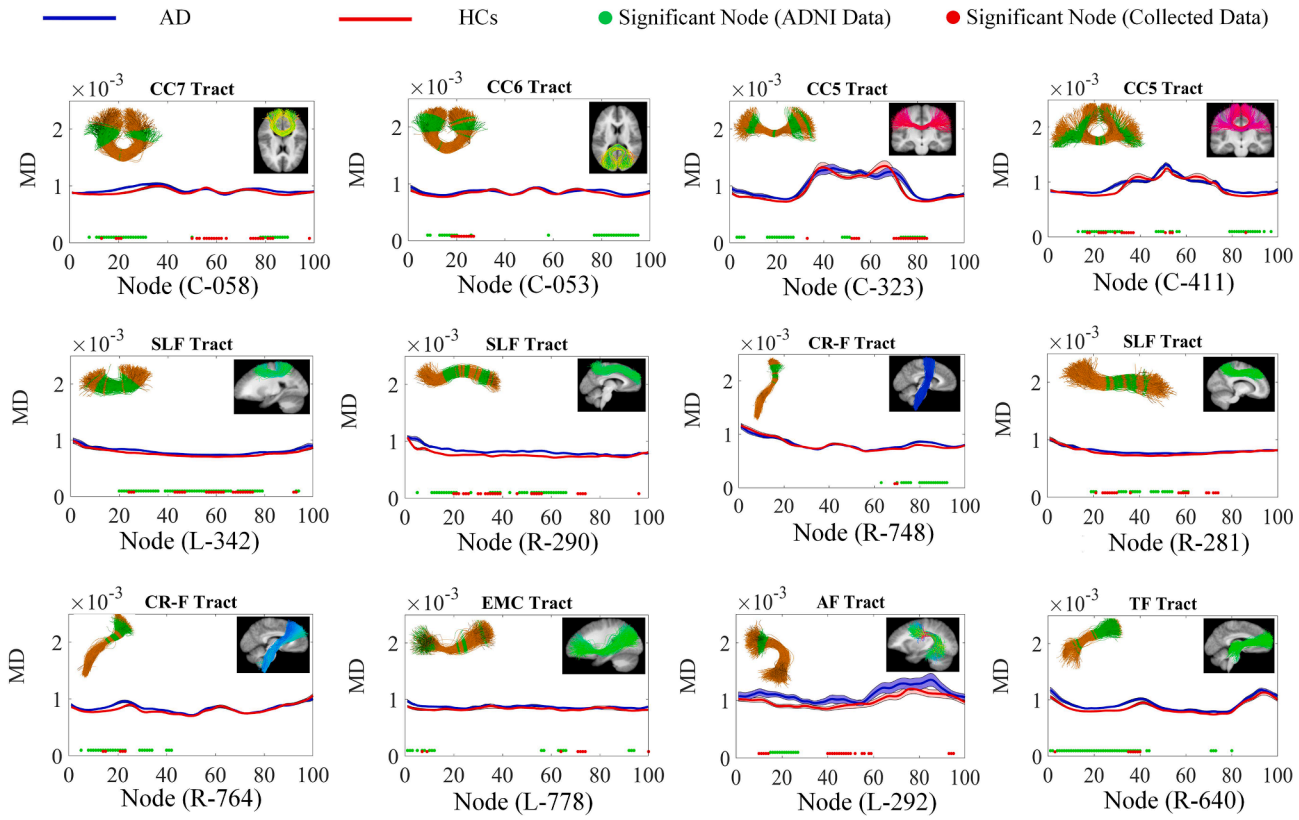

Fig. 3. Significant differences MD in AD group on two datasets. The green dots show the significant difference nodes on ADNI dataset. The red dots show the significant difference nodes on collected dataset. The blue and red curves show the profiles of AD and HCs on ADNI dataset.

2.3.5. *Group profiles computation*

For all the points in a bundle, we can get the FA and MD values directly from the DTI image. FC was a macroscopic index that can reflect the change of bundle cross-section. The direction should be consistent with current fiber's direction d_{fiber}. We selected the FC value that had smaller angle with fiber's direction as the measure. After the properties of each node were obtained, the corresponding values in the same node were averaged. The properties of each node included three measures, that were FA, MD, and FC. The anatomical measures along with a fiber bundle was commonly referred as bundle profile [10–12]. The measure of each bundle of ClusterMetric was a vector with 3 rows and m columns, where m was the number of nodes within a bundle.

3. Experiments and results

In this work, we summarized the fiber bundle measures (FA, MD, and FC) along with the length of each cluster using the proposed ClusterMetric. Then, we conduct the Mann-Whitney U-tests for not normally distributed variables and the unpaired t-test for normally distributed variables to find the group-wise significant differences on both datasets.

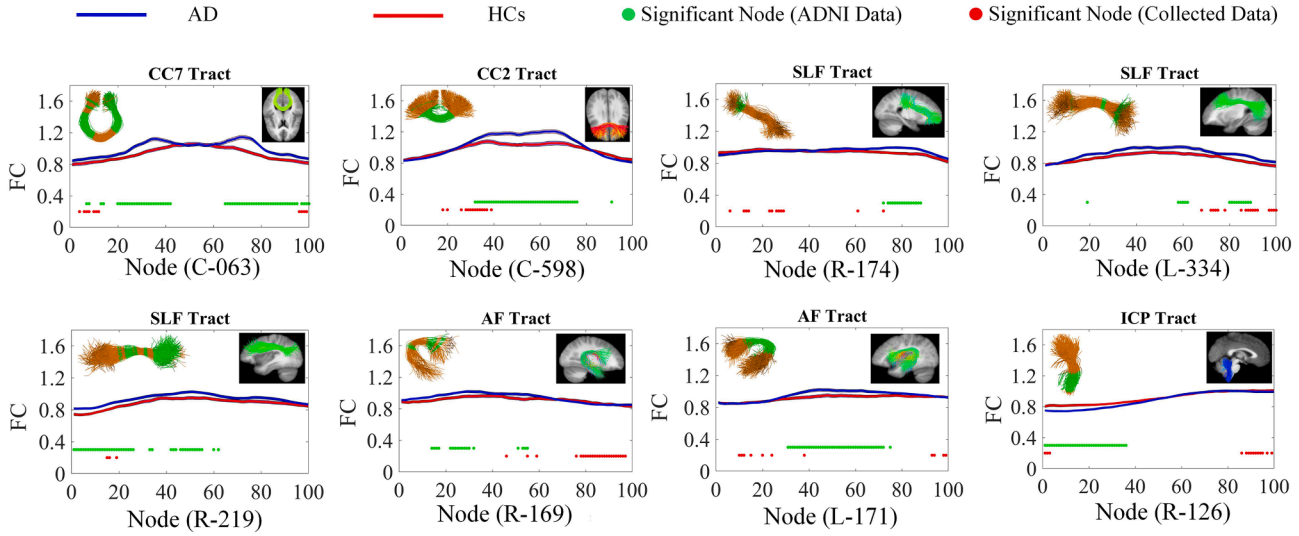

Fig. 4. Significant differences FC in AD group compared to HCs on two datasets. The green dots show the significant difference nodes on ADNI dataset. The red dots show the significant difference nodes on collected dataset. The blue and red curves show the profiles of AD and HCs on ADNI dataset.

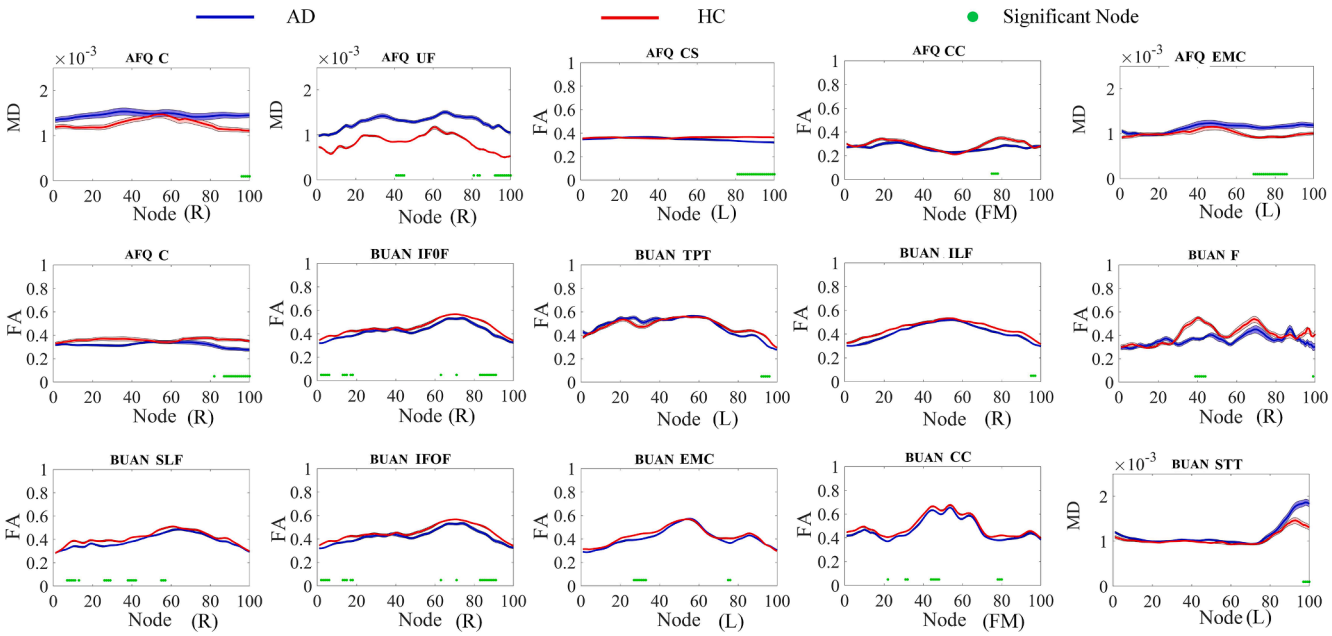

Fig. 5. The comparisons between AD and HCs groups using AFQ and BUAN methods on our collected AD dataset. L and R: left and right hemispheres; FM: ForcepsMajor of the corpus callosum; C: Cingulum; CS: Corticostriatal Tract; STT: Spinothalamic Tract; TPT: Temporopontine Tract; ILF: Inferior Longitudinal Fasciculus; F: Fornix.

Multiple comparisons were corrected across all 100 nodes on each cluster using the FDR at $p< 0.05$. To contrast and cross-validate the performance of proposed ClusterMetric, we also performed group-wise comparisons using the AFQ and BUAN methods on our collected dataset.

Fig. 2 depicted the group-wise differences using anatomical measures of the FA along with the cluster at specific locations on two datasets. We found significant FA decrease in AD group in multiple clusters, which were distributed in CC, superior longitudinal fasciculus (SLF), inferior occipito-frontal fasciculus (IoFF), cingulum bundle (CB), TF, uncinate fasciculus (UF), and extreme capsule (EMC). The cluster C-404 and C-621 belonging to CC forceps showed significantly decreased FA on both datasets. The cluster R-465 (CB) and R-682 (CB) showed FA decrease largely. The cluster R-769 (IoFF) and R-752 (IoFF) showed FA decrease at close anatomical locations. The cluster L-236 (SLF) and R-216 (SLF) showed FA decrease nearby 20th and 80th node.

Statistically significant differences between the groups were found in MD along with the CC, SLF, corona-radiata-frontal (CR-F), arcuate fasciculus (AF), TF, and EMC tracts as shown in Fig. 3. Cluster C-058 (CC7) belonging splenium of CC. Cluster C-053 (CC6), C-323 (CC5) and C-411 (CC5) belonging trunk of CC show significantly increased MD in AD group. Cluster L-342 (SLF), R-290 (SLF), and R-281 (SLF) show MD increase at the middle part of the clusters in AD group.

Fig. 4 showed decreased FC in AD group within the eight clusters, which were distributed in CC, AF, inferior cerebellar peduncle (ICP), and SLF tracts. The FC was computed by the deformation field from template to individual space. Accordingly, the bundle cross-section degeneration signified a large FC value as the measure of deformation was from the large cross-section to the small cross-section. We observed FC decrease in cluster C-063 (CC7) belonging to splenium of CC in AD group. Cluster C-598 (CC2) showed FC decrease at the genu of CC. Cluster L-334 (SLF) showed FC decrease at the ending location along with the bundle on both datasets.

The existing methods of AFQ and BUAN were performed to cross-validate the findings (Fig. 5). Significantly decreased FA was also observed in CC tract in AD group with both methods. We also found decreased FA in right cingulum tract with AFQ method, which was consistent with the proposed method (R-465 and R-682). The increased MD was found in left EMC tract in AD group with AFQ methods, which was also observed in cluster L-778 (EMC). The decreased FA in right SLF with BUAN methods was consistent with cluster R-216 (SLF). In addition, the decreased FA in IFOF with BUAN methods was also consistent with cluster R-769 (IoFF) and R-752 (IoFF). The increased MD in STT with BUAN method was also observed in cluster R-640 (TF).

The partial correlation of anatomical measures with MMSE score was shown in Fig. 6. The fiber measures were considered to be related to MMSE scores when R-values were greater than 0.3 and P-values were less than 0.05 simultaneously for both datasets within the significant nodes. We observed cluster L-292-MD (AF), C-598-FC (CC2), C-323-MD (CC5), C-411-MD (CC5), and L-342-MD (SLF) were negatively correlated with MMSE scores. Moreover, we found that the FA in cluster C-466 was positively correlated with MMSE scores.

4. Discussion

In this study, the proposed ClusterMetric used a data-driven based fiber parcellations and node identification pipeline to summarize the fiber properties along with the length of cluster. The proposed method combined FA, MD, and FC to evaluate white matter changes at the microscopic and macroscopic levels. Compared with previous tractometry methods such as AFQ [12] and BUAN [10], the nodes identified by ClusterMetric were more consistent across subjects. Compared to the previous FC algorithm, the ClusterMetric did not need professional anatomical knowledge for fiber bundle annotation [25–26]. The ClusterMetric was available with detailed steps including dMRI tractography, fiber parcellation, node identification, bundle profile computation, statistical comparisons across groups, and result expression. We hoped the pipeline can simplify the calculation with complex indicators such as FC profile, and facilitate exploratory dMRI investigations.

Furthermore, we applied the ClusterMetric to our collected dataset including 23 AD subjects and 22 HCs and ANDI dataset including 53 AD subjects and 85 HCs. The results showed significantly changed white matter clusters belonging to multiple tracts on both datasets. Notably, we found the fiber measures in part of the significant clusters were correlated with the MMSE scores. The findings were consistent with previous studies that the FA values of the SLF, IoFF, CB, UF, TF, EMC,

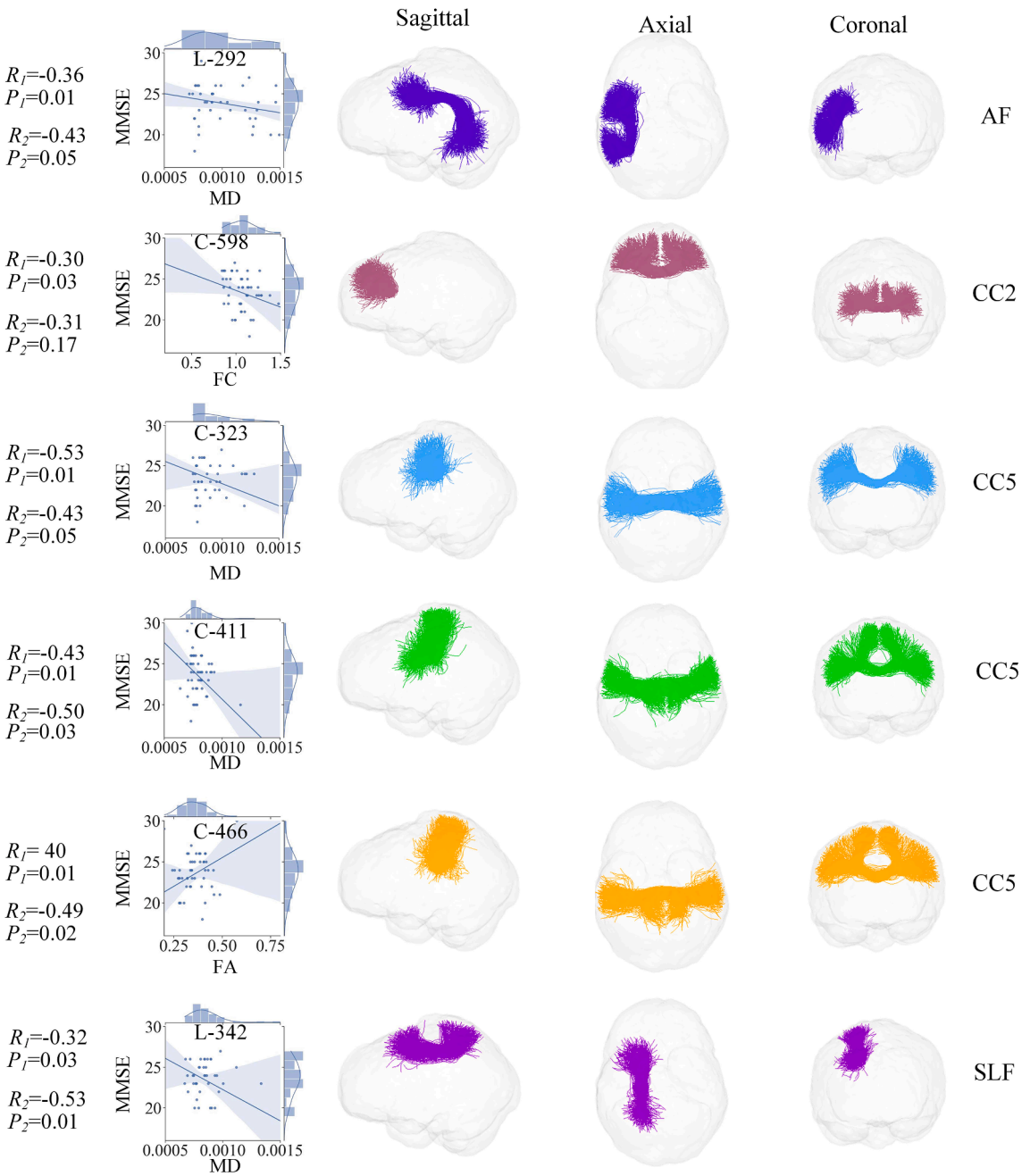

Fig. 6. Correlation of anatomical measures in significant difference nodes with MMSE scores. A partially transparent model of the brain is shown as a background to describe the relative position of each cluster. We verify the correlation on ANDI dataset (R_1 and P_1) and collected dataset (R_2 and P_2). The scatter figures show anatomical measures and MMSE scores in significantly different nodes with the maximum R-value within a cluster on ANDI dataset.

and CC decreased significantly, as well as MD values showed significant increase within CC, SLF, CR-F, EMC, AF, and TF tracts in AD group compared to HCs [20,27–29]. Moreover, the FC values were significantly decreased at specific locations along the length of these clusters belonging to the CC, SLF, ICP, and AF tracts in AD groups compared to the HCs, which was rarely mentioned in previous studies. As suggested by previous studies, these fiber tracts connected brain areas that had been considered functional damage and structural degeneration in AD. Here, the proposed method may enable a comprehensive insight into white matter changes and offer novel perspectives into the degenerative changes to fiber pathways in these clinical disease states.

This study had several limitations. Firstly, the sample size of collected dataset was relatively small, which collected 45 subjects. Secondly, the node identification algorithm in ClusterMetric may face a challenge when the bundle shapes were very difficult to summarize. Thirdly, the samples contained both early- and late-onset cases. Separating early- and late-onset AD in the analysis was meaningful in the future work.

5. Conclusion

The proposed ClusterMetric realized automatic parcellation of whole brain tractogram and automatic annotation of distorted white matter on a finer scale. Our application on two datasets suggested that the AD group exhibited a characteristic pattern of fiber tract degeneration, which manifested both as microstructural and macrostructural changes in white matter. The pattern of changes in structural connectivity was consistent with previous literatures, and our findings provided a more

subtle scale in abnormal white matter location. We hoped the Cluster-Metric can facilitate the understanding of the pathogenic mechanisms in neurological diseases and neuroplasticity studies.

CRediT authorship contribution statement

Jingqiang Wang: Investigation, Methodology, Writing – original draft, Writing – review & editing. **Caiyun Wen:** Conceptualization, Investigation, Validation, Writing – original draft, Writing – review & editing. **Jinwen Li:** Investigation, Methodology, Formal analysis. **Jianhe Chen:** Resources, Writing – review & editing, Supervision. **Yuanjing Feng:** Conceptualization, Project administration, Resources, Supervision.

Declaration of Competing Interest

The authors declare that they have no known competing financial interests or personal relationships that could have appeared to influence the work reported in this paper.

Acknowledgments

This study was supported by the National Natural Science Foundation of China [grant No. (61976190, 61903336]; Key Research & Development Project of Zhejiang Province, China [grand, No. 2020C03070]; Major Science and Technology Projects of Wenzhou, China [grant No. ZS2017007]; The Wenzhou Municipal Science and Technology Bureau, China [grant No. Y2020062].

Appendix A. Supplementary data

Supplementary data to this article can be found online at https://doi.org/10.1016/j.neulet.2022.136724.

References

[1] P.J. Basser, J. Mattiello, D. LeBihan, MR diffusion tensor spectroscopy and imaging, Biophys. J. 66 (1) (1994) 259–267, https://doi.org/10.1016/S0006-3495(94)80775-1.
[2] J.S. Shimony, R.C. McKinstry, et al., Quantitative diffusion-tensor anisotropy brain MR imaging: normative human data and anatomic analysis, Radiology 212 (1999) 770–784, https://doi.org/10.1148/radiology.212.3.r99au51770.
[3] P.J. Basser, S. Pajevic, et al., In vivo fiber tractography using DT-MRI data, Magn. Reson. Med. 44 (4) (2015) 625–632, https://doi.org/10.1002/1522-2594(200010)44:43.0.CO;2-O.
[4] S. Farquharson, J.D. Tournier, F. Calamante, et al., White matter fiber tractography: why we need to move beyond DTI, J. Neurosurg. 118 (6) (2013) 1367–1377, https://doi.org/10.3171/2013.2.JNS121294.
[5] P. Guevara, D. Duclap, C. Poupon, et al., Automatic fiber bundle segmentation in massive tractography datasets using a multi-subject bundle atlas, Neuroimage 61 (4) (2012) 1083–1099, https://doi.org/10.1016/j.neuroimage.2012.02.071.
[6] L.J. O'Donnell, C.F. Westin, et al., The fiber laterality histogram: a new way to measure white matter asymmetry, in: In: International Conference on Medical Image Computing and Computer-assisted Intervention (MICCAI), 2010, pp. 225–232, https://doi.org/10.1007/978-3-642-15745-5_28.
[7] H. Johansen-Berg, T.E. Behrens, Just pretty pictures? What diffusion tractography can add in clinical neuroscience, Curr. Opin. Neurol. 19 (4) (2006) 379–385, https://doi.org/10.1097/01.wco.0000236618.82086.01.
[8] Y. Wu, F. Zhang, N. Makris, et al., Investigation into local white matter abnormality in emotional processing and sensorimotor areas using an automatically annotated fiber clustering in major depressive disorder, Neuroimage 181 (2018) 16–29, https://doi.org/10.1016/j.neuroimage.2018.06.019.
[9] F. Zhang, Y. Wu, I. Norton, et al., An anatomically curated fiber clustering white matter atlas for consistent white matter tract parcellation across the lifespan, NeuroImage 179 (2018) 429–447, https://doi.org/10.1016/j.neuroimage.2018.06.027.
[10] B.Q. Chandio, S.L. Risacher, F. Pestilli, et al., Bundle analytics, a computational framework for investigating the shapes and profiles of brain pathways across populations, Sci. Rep. 10 (1) (2020) 17149, https://doi.org/10.1038/s41598-020-74054-4.
[11] J.D. Yeatman, R.F. Dougherty, N.J. Myall, B.A. Wandell, H.M. Feldman, Tract profiles of white matter properties: automating fiber-tract quantification, PLoS One 7 (11) (2012) e49790.
[12] J.D. Yeatman, A. Richie-Halford, J.K. Smith, A. Keshavan, A. Rokem, A browser-based tool for visualization and analysis of diffusion MRI data, Nat. Commun. 9 (1) (2018) 940, https://doi.org/10.1038/s41467-018-03297-7.
[13] Y. Feng, J. Song, W. Yan, J. Wang, C. Zhao, Q. Zeng, Investigation of Local White Matter Properties in Professional Chess Player: A Diffusion Magnetic Resonance Imaging Study Based on Automatic Annotation Fiber Clustering, IEEE TCDS 13 (2) (2021) 403–415, https://doi.org/10.1109/TCDS.2020.2968116.
[14] J.D. Tournier, R.E. Smith, D. Raffelt, et al., A. MRtrix3: A fast, flexible and open software framework for medical image processing and visualisation, NeuroImage 202 (2019), https://doi.org/10.1016/j.neuroimage.2019.116137.
[16] E. Garyfallidis, M.A. Cote, F. Rheault, et al., Recognition of white matter bundles using local and global streamline-based registration and clustering, Neuroimage 170 (2018) 283–295, https://doi.org/10.1016/j.neuroimage.2017.07.015.
[17] D.A. Raffelt, R.E. Smith, G.R. Ridgway, et al., Connectivity-based fixel enhancement: Whole-brain statistical analysis of diffusion MRI measures in the presence of crossing fibres, Neuroimage 117 (2015) 40–55, https://doi.org/10.1016/j.neuroimage.2015.05.039.
[18] D.A. Raffelt, J.D. Tournier, R.E. Smith, et al., investigating white matter fibre density and morphology using fixel-based analysis, NeuroImage 144 (2017) 58–73, https://doi.org/10.1016/j.neuroimage.2016.09.029.
[19] X. Dou, H. Yao, F. Feng, et al., Characterizing white matter connectivity in Alzheimer's disease and mild cognitive impairment: An automated fiber quantification analysis with two independent datasets, Cortex 129 (2020) 390–405, https://doi.org/10.1109/ISBI.2019.8759211.
[20] Q. Zhao, H. Lu, H. Metmer, W. Li, J. Lu, Evaluating functional connectivity of executive control network and frontoparietal network in Alzheimer's disease, Brain Res. 1678 (2018) 262–272, https://doi.org/10.1016/j.brainres.2017.10.025.
[21] MM, Bozzali, A, Falini, M, Franceschi, M.uffi. M. Cercignani, G. Scotti, G. Comi, M. Filippi, White matter damage in alzheimer's disease assessed in vivo using diffusion tensor magnetic resonance imaging, J. Neurol. Neurosurg, Psychiatry, 42 (2002) 742-746. 10.1136/jnnp.72.6.742.
[22] B.B. Avants, N. Tustison, G. Song, Advanced normalization tools (ANTS), Insight Journal 2 (2009) 1–35, https://doi.org/10.1007/978-3-319-14678-2_1.
[23] J.G. Malcolm, M.E. Shenton, Y. Rathi, Filtered multitensor tractography, IEEE Trans. Med. Imaging 29 (9) (2010) 1664–1675, https://doi.org/10.1109/tmi.2010.2048121.
[24] J.D. Tournier, F. Calamante, A. Connelly, Robust determination of the fibre orientation distribution in diffusion MRI: non-negativity constrained super-resolved spherical deconvolution, Neuroimage 35 (4) (2007) 1459–1472, https://doi.org/10.1016/j.neuroimage.2007.02.016.
[25] K. Pannek, J. Fripp, J.M. George, et al., Fixel-based analysis reveals alterations is brain microstructure and macrostructure of preterm-born infants at term equivalent age, Neuroimage Clin 18 (2018) 51–59, https://doi.org/10.1016/j.nicl.2018.01.003.
[26] S.W. Choy, E. Bagarinao, H. Watanabe, et al., Changes in white matter fiber density and morphology across the adult lifespan: A cross-sectional fixel-based analysis, Hum. Brain Mapp. 41 (12) (2020) 3198–3211, https://doi.org/10.1002/hbm.25008.
[27] Y. Zhang, N. Schuff, et al., Diffusion tensor imaging of cingulum fibers in mild cognitive impairment and Alheimer disease, Neurology 68 (1) (2007) 13–19, https://doi.org/10.1212/01.wnl.0000250326.77323.01.
[28] R.H. Yin, L. Tan, Y. Liu, et al., Multimodal voxel-based meta-analysis of white matter abnormalities in Alzheimer's disease, J. Alzheimers Dis. 47 (2) (2015) 495–507, https://doi.org/10.3233/jad-150139.
[29] S.H. Lee, J.P. Coutu, P. Wilkens, A. Yendiki, H.D. Rosas, D.H. Salat, Tract-based analysis of white matter degeneration in Alzheimer's disease, Neuroscience 301 (2015) 79–89, https://doi.org/10.1016/j.neuroscience.2015.05.049.